

See discussions, stats, and author profiles for this publication at: <https://www.researchgate.net/publication/252230775>

Quasi-optical verification of the focal plane optics of the Heterodyne Instrument for the Far-Infrared (HIFI)

Article in *Proceedings of SPIE - The International Society for Optical Engineering* · September 2004

DOI: 10.1117/12.551144

CITATIONS

2

READS

32

8 authors, including:



Massimo Candotti

42 PUBLICATIONS 95 CITATIONS

[SEE PROFILE](#)



Willem Jellema

Netherlands Institute for Space Research, Utrecht

114 PUBLICATIONS 1,670 CITATIONS

[SEE PROFILE](#)



John Lavelle

Danish Meteorological Institute

17 PUBLICATIONS 102 CITATIONS

[SEE PROFILE](#)



John Anthony Murphy

National University of Ireland, Maynooth

379 PUBLICATIONS 18,924 CITATIONS

[SEE PROFILE](#)

Some of the authors of this publication are also working on these related projects:



Automatic Sea Ice Products [View project](#)



ALMA band 9 [View project](#)

Quasi-Optical Verification of the Focal Plane Optics of the Heterodyne Instrument for the Far-Infrared (HIFI)

Candotti M.^a, Cahill G.^a, Finn T.^a, Jellema W.^b, Lavelle J.^a, Murphy J. A.^a, O'Sullivan C.^a,
Trappe N. A.^a.

^aNational University of Ireland Maynooth (NUIM), Exp. Physics Dep., Maynooth, Co.
Kildare, Ireland;

^bSpace Research Organization of the Netherlands (SRON), P.O.Box 800, 9700 AV Groningen,
the Netherlands.

ABSTRACT

HIFI is one of the three instruments for the Herschel Space Observatory, an ESA cornerstone mission. HIFI is a high resolution spectrometer operating at wavelengths between 157 and 625 μm . The need for a compact layout reducing the volume and mass as much as possible has important consequences for the optical design. Many mirrors are located in the near-field of the propagating beam. Especially in the long wavelength limit diffraction effects might therefore introduce significant amplitude and phase distortions. A classical geometrical optical approach is consequently inadequate. In this paper we present a rigorous quasi-optical analysis of the entire optical system including the signal path, local oscillator path and onboard calibration source optical layout.

In order to verify the results of the front-to-end coherent propagation of the detector beams, near-field measurement facilities capable of measuring both amplitude and phase have been developed ¹. A remarkable feature of these facilities is that the absolute coordinates of the measured field components are known to within fractions of a wavelength. Both measured and simulated fields can therefore be compared directly since they are referenced to one single absolute position.

We present a comparison of experimental data with software predictions obtained from the following packages: GRASP* (Physical Optics Analysis) and GLAD[†] (Plane Wave Decomposition).

We also present preliminary results for a method to correct for phase aberrations and optimize the mirror surfaces without changing the pre-designed mechanical layout of the optical system.

Keywords: experimental verification, far-infrared, near-field, beam propagation, electromagnetic simulations.

1. INTRODUCTION

In this paper we investigate, by means of software simulations and experimental measurements, the performances of the HIFI front end. HIFI is a heterodyne spectrometer instrument due for launch in 2007 on the Herschel Space Telescope (an European Space Agency (ESA) satellite). This instrument will allow astronomers to observe using the last major unutilised part of the electromagnetic spectrum (wavelengths from 100 microns to 1 millimetre). That means the instrument will provide continuous coverage over the frequency range from 480 – 1120 GHz in five bands and from 1410 – 1910 GHz in two additional bands. For the five lower bands a Superconductor Insulator Superconductor (SIS) mixer detectors will be used. For the remaining higher bands the mixers will be Hot Electron Bolometers (HEB). In each band a set of orthogonal polarized mixers will operate, being coupled to the sky and local oscillator signal by means of a corrugated horn from band 1 to 4 and a lens antenna for the remaining higher bands ².

The second section gives a brief and essential description of the Focal Plane Unit (FPU) specifying the related detail of each modular block composing it. A general guideline on how this coupling system was designed

Send correspondence to

Massimo Candotti: E-mail: massimo.candotti@may.ie, Telephone: +353 1 708 3552.

*©TICRA.

[†]©Applied Optics Research.

is described. In fact most of the scatterers are positioned in the system in the near field region and in order to achieve a compact design, off-axis reflectors are often used. Both these two characteristics of the system design imply, especially at the longer wavelengths, aberration and general distortion of both amplitude and phase of the propagating beam. The longest wavelength will suffer larger aberrations as it is furthest from the geometric limit. It is therefore necessary to concentrate analysis on the longest wavelength channel as the worst aberrations are expected there. For that reason the frequency of the following results is referred to be 480 GHz or equivalently in term of wavelength $0.625\ \mu\text{m}$.

In the third section a description of the main characteristic of the experimental measurement setup is reported, with a concise explanation on how the system works. A concise summary of the system accuracy.

Section 4 explains the capabilities of the commercial software packages used in our work (GLAD and GRASP), giving some details about the approximations introduced by these software in calculating the electromagnetic fields.

In order to achieve results as close as possible to the reality, noticeable attention should be take into account on the right source definition. For that, section 5 clarify how the corrugated horn was modelled in our software predictions.

The comparison of the results taken in four positions of the FPU are shown and discussed in section 6 in order to investigate the comparison between theory prediction and measurement.

In section 7, we discuss an optimization process to improve the beam quality at an output plane of HIFI by changing the surface of an intermediate field mirror by correcting the phase error on the surface of the mirror. We report on the analytical technique used and report on beam quality improvements obtained.

Finally the conclusions are presented. Accuracy of the software predictions and measurements are discussed highlighting possible causes of disagreement between the compared data.

2. HIFI FOCAL PLANE OPTICS DESCRIPTION

The HIFI focal plane optics can be divided in four sub-assemblies ³. The main component is the Common Optics Assembly (COA) from which the telescope signal is re-imaged to the 7 channels, see figure 1. The optical train can be divided into wavelength independent parts which are then merged together to form the complete optical path. Two Mixer Sub-Assemblies (MSA) are used on each channel to allow simultaneous measurement of the Vertical and Horizontal Polarization (VP and HP) as the mixer devices are only sensitive to one field component, figure 1b). The Cold Local oscillator Optics assembly (CLO) is a wavelength independent mirror coupling system identical for each channel, figure 1d), which purpose is to couple the LO beam, coming through a cryostat windows, to the MSA 1d). The fourth component of the system is the Calibration Sub-Assembly (CSA). The function of the COA, figure 1a) and 1c), is to relay the field of view of the Herschel telescope to the 7 pairs of MSAs by means of a two stage re-imaging system, figure 1b). A chopper mirror is used within the COA and its rotation allows the mixer to observe the the sky or the onboard "hot" and "cold" black body in the CSA. Since HIFI is a heterodyne instrument a local oscillator (LO) beam has to be directed to each MSA. The MSA combines for each channel the beam from the telescope and from the CLO and send those coinciding beams to two orthogonal mixer units. A Martin-Puplett interferometer type set up for channels 3-7 and a beamsplitter configuration for the lower bands is used to combine the beams from the sky and the LO. The mixer antennas for channels 1 - 4 are circular corrugated horns, while in channels 5, 6a and 6b double dipole microstrip antenna at the back of a hyper-hemispherical silicon lens are used.

The optical blocks are designed to be wavelength independent. Dispersion in the design is avoided by the exclusive use of mirrors. Wavelength dependency in the Gaussian Mode optical sense means that in general both the position and size of an imaged waist is wavelength dependent.

In order to achieve a modular optical design each block of the FPU was thought to interface with another one by means of a wavelength independent beam waist and radius of curvature in a so-called geometrically conjugated plane. For instance if a Gaussian waist is located in one of these planes (object), both the curvature and size of the resulting Gaussian wavefront in another such a plane (image) is invariant for wavelength through the action of any intervening optical system.

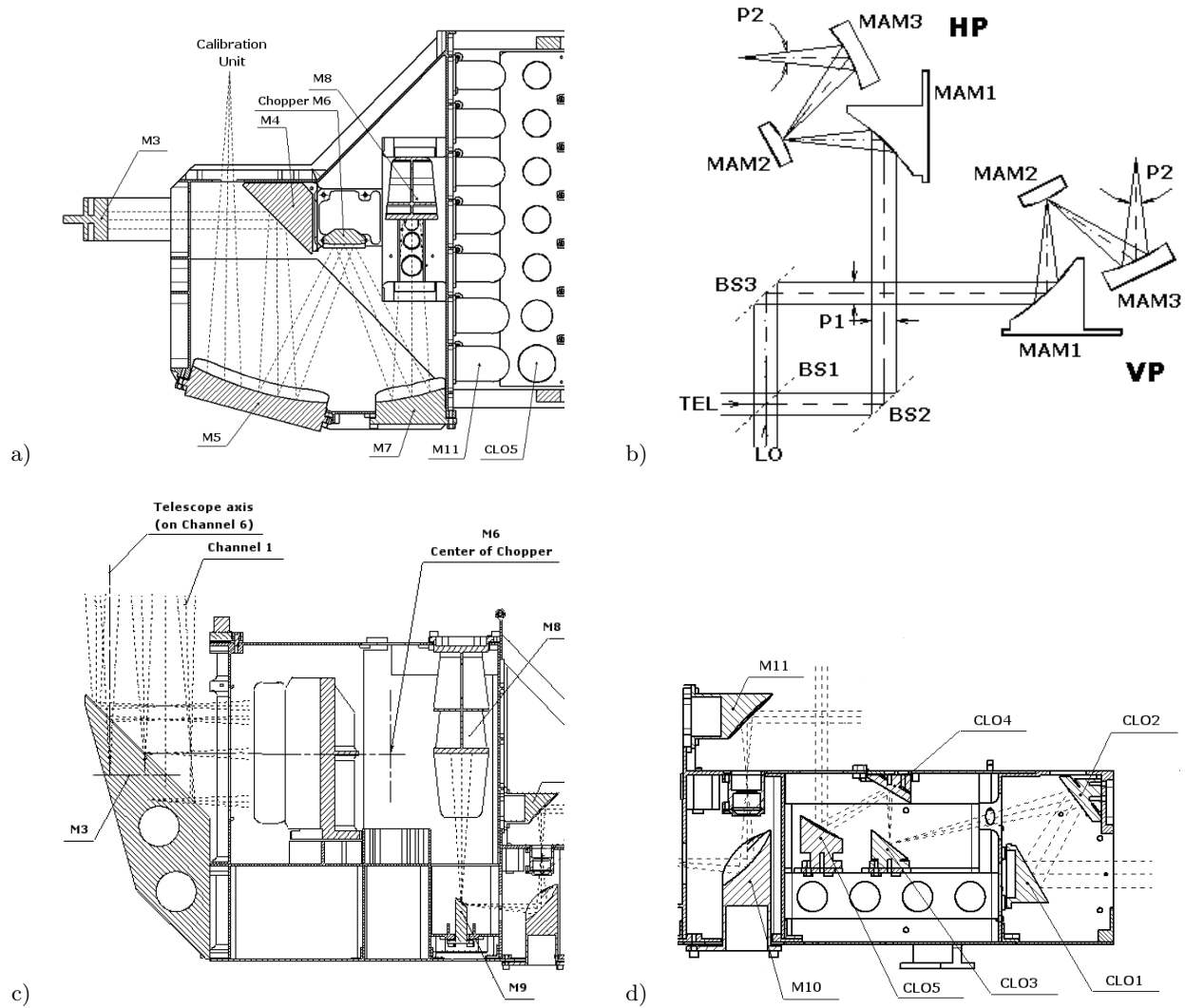


Figure 1. HIFI optical system cross sections ³. a) COA telescope axis normal plane, b) MSAs telescope on-axis plane, c) COA telescope on-axis plane, d) CLO telescope on-axis plane.

In the design of the FPU there are two sets of conjugated planes:

- The pupil planes (P1) as indicated above. These planes are all conjugated to the system aperture stop (Secondary Mirror).
- The image planes. These are the planes in which the sky is imaged (e.g. telescope focal plane and channel splitting mirrors).

The design is laid out such that in each of the optical blocks an image plane is located. At these image planes so-called field mirrors are positioned. In optical systems field mirrors are used to control the imaging of pupil planes. In the present design the optical power of the field mirrors is used to ensure that the interface planes coincide with the pupil images.

3. NEAR FIELD MEASUREMENT FACILITY AND DEVICE UNDER TEST

The measurement setup located at the SRON laboratories in Groningen, is a scanning system capable of performing planar near-field antenna measurement ¹. The receiving antenna is scanned over an uniformly spaced grid located at the output of corrugated horn transmitting device (generally consisting of the transmitting antenna and the reflective optics associated with it). Both amplitude and phase are recorded for each point on the grid at a defined polarization. In order to preserve the phase information the measurement system is based on radio heterodyne detection method employing a vector analyzer and external microwave circuitry. The scanning system consists of two linear stages mounted orthogonal to each other and driven by two linear motors. The detector is then able to move on this plane within a square whose dimensions and accuracy resolution are shown in table 1. The linear polarized detector can also be rotated by 90° or 180° allowing co- and cross-polar pattern measurements. A detailed description of this system has been given in ¹. A summary of the electrical characteristics is shown in table 1. The alignment operations are made with a dedicated setup in order to relate

Table 1. Main characteristics of the scanning system.

Electrical parameters	Value	Scanner range & resolution parameters	Value
Frequency of operation [GHz]	480	Scanning range in x [mm]	100
Signal to Noise Ratio (SNR) [dB]	60	Scanning range in y [mm]	75
IF bandwidth B [Hz]	10	Scanning range in z [mm]	75
Integration time τ [s]	0.1	On-axis position resolution [μ]	± 5
Amplitude stability [%/hr]	± 2	Alignment accuracy parameters	Value
Phase stability [$^{\circ}$ /hr]	± 20	Lateral offset in x and y [mm]	< 0.1
Residual gain compression [dB]	< 0.3	Axial offset in z [mm]	< 0.2
Typical 1σ main beam ampl. error [dB]	0.5	Tilt around x and y [arcmin]	< 5
Typical 1σ main beam phase error [$^{\circ}$]	10	Tilt around z [$^{\circ}$]	< 0.1

the internal alignment of the instrument to the external mechanical interfaces. The alignment operations are based on theodolite autocollimation procedures. The overall alignment accuracy obtained is shown in table 1. Following this alignment methodology it is possible to have measured and simulated data both referenced to one single absolute position in relation to a common chosen co-ordinate system.

4. DESCRIPTION OF THE SOFTWARE PACKAGES

We shall now provide a brief description of the basic operations of the packages used for predicting the electromagnetic fields. First however, we would like to emphasize that this presentation should not be considered as a full description of all the features or capabilities of the package.

4.1. GLAD (General Laser Analysis and Design)

GLAD is software package designed to calculate system performance of optical systems that have a well-defined direction of propagation. GLAD represents the optical beam as the complex amplitude of the optical wave-front. This is unlike geometrical optics, which represents the beam as geometrical rays. GLAD then uses Plane Wave decompositions to propagate the beam through free-space and ray traces through components to determine the aberration function, the Optical Path Difference (OPD).

Rather than evaluating diffraction integrals directly, it is possible to decompose the assumed source field into modes and then propagate the modes as required. Propagating modes through free space is usually straightforward and often simply consists of taking into account the mode phase slippage with respect to each other. One of the most attractive schemes is to break the field down into plane waves ⁴. Plane waves are exact solutions of the Helmholtz equation, and therefore the only assumptions made relate to the field across the source plane. A plane wave analysis has the significant advantage that it is not limited to paraxial fields unlike Gaussian modes, which on the other hand, are solutions of the paraxial wave equation, although GLAD still limits the plane wave equation to paraxial field as it is a scalar package and assumes little or no deviation from the paraxial approximation ⁶.

The performance of GLAD has been optimized for shorter wavelengths rather than those typically found in sub-millimetre astronomy. It is also limited by the fact that it does not automatically calculate aperture efficiencies or coupling efficiencies as well as neglecting cross-polarization, all critical parameters in determining system performance and optimization in sub-millimetre systems. GLAD defines the real aperture rims by positioning an aperture contour in the plane of the optical component, giving a more effective approximation of edge diffraction. GLAD has its own user defined Gaussian which can be propagated through the system. It is also possible to input a user defined field distribution to GLAD such as that radiated by a conical corrugated horn. This allows for a more representative view of the optical relay.

4.2. GRASP (General Antenna Full Electromagnetic Analysis)

The electromagnetic analysis conducted using GRASP is based on Physical Optics (PO) theory applied to scattering problems⁵. In general a scattering problem consists of a known incident field and a scatterer with known geometry and electrical surface properties. The total radiated field at a given distance R from the origin \bar{E} , could in general be thought as the sum of an incident field \bar{E}^i and the related scattered field \bar{E}^s , $\bar{E} = \bar{E}^i + \bar{E}^s$. If the surfaces of the conductor are perfectly conducting the scattered field is generated by the induced surface current on the scatterer. The scattering analysis can thus be considered as a three step procedure where the first step is to calculate the induced or equivalent surface currents, the second step is to calculate the radiated field by these currents and the third step is to add the incident and scattered fields to obtain the total field. The PO method gives an approximation to the surface currents valid for perfectly conducting scatterers which are large in terms of wavelengths. Within this approximation it is assumed that the surface current at a specific point on a curved, but perfectly conducting scatterer, is the same as the surface current on an infinite planar surface which is tangent to the scattering surface at this point.

The induced currents on a perfectly conducting infinite plane surface illuminated by an arbitrary incoming field are given by well known formula $\bar{J}^e = 2\bar{n} \times \bar{H}^i$ which constitutes the PO approximation, where \bar{J}^e is the induced electric current, \bar{n} is the unit normal (pointing outward on the illuminated side of the surface) and \bar{H}^i is the incident magnetic field.

Once obtained the equivalent currents, electric and magnetic fields are calculated from the vector potential \bar{A}^e yielding⁵:

$$\bar{A}^e = \frac{\mu_0}{4\pi} \int \int_B \bar{J}^e(\bar{r}') \frac{\exp^{-jkR}}{R} ds', \quad \bar{E}^e = -j\omega\bar{A}^e + \frac{\nabla(\nabla \cdot \bar{A}^e)}{j\omega\mu_0\epsilon_0}, \quad \bar{H}^e = \frac{1}{\mu_0} \nabla \times \bar{A}^e. \quad (1)$$

where ϵ_0 and μ_0 are the free space permittivity and the permeability, respectively. The parameter ω is the angular frequency and $k = 2\pi/\lambda$ is the wavenumber. The distance R is given by $R = |\bar{r} - \bar{r}'|$ where \bar{r} is the position of the observation point and \bar{r}' is the integration variable running over the surface. The subscription B denotes integration over the scattering surface.

The electric and magnetic fields are calculated by numerical integration of the equations above, but in order to obtain an efficient procedure these surface integrals are computed by a standard two-dimensional integration on a plane by means of an integral transformation procedure.

Finally some points must be considered. Despite the PO current radiation being done rigorously according to Maxwell equations, the PO method should only be used if the dimensions of the scattering surface and its radius of curvature are sufficiently large measured in wavelengths. For simple surface shapes PO is often used for scatterers down to five wavelength in diameter. The PO approximation neglects the non-uniform currents near the edge of the scatterer. However GRASP takes into account of these effects using the "Physical Theory of Diffraction" (PTD). Further the full electromagnetic vector analysis carried out by GRASP allows one to obtain all kinds of information related to a scattered field (co-polar, cross-polar, spill-over, beam efficiency, etc.).

5. BAND 1 CORRUGATED HORN INPUT FIELD MODEL

As indicated in section 2 the mixer antennas for channel 1 is a circular corrugated horn. To input a representative field of the antenna and arbitrary aperture field is entered.

According to ⁶ an r-directed linear polarized electric field distribution at the aperture of a corrugated horn can be described by

$$\bar{E}_{ap}(r) = J_0\left(\frac{2.405r}{a}\right) \exp\left(\frac{-jr^2}{\lambda R_h}\right) \hat{r} \quad r \leq a. \quad (2)$$

where J_0 is a zeroth order Bessel function, a is the aperture radius, r is the radial distance from the horn axis and 2.405 is the first zero of J_0 . The exponential term represent the spherical wave phase having a radius of curvature equal to R_h , the horn slant length. This beam shape is a good approximation of a conical corrugated horn field, taking into account that this pure linear polarization model agrees quite well with the excellent polarization properties of a corrugated feed.

In order to describe the aperture field of the corrugated horn in use for band 1, the design parameter of slant length $R_h = 15.4mm$ and an aperture radius $a = 2.5mm$ were taken.

6. COMPARISON OF THE RESULTS

In this section we will consider three planes of comparison between measured and simulated results plus the incident beam pattern on the two black bodies of the CSA. The three planes were chosen to be the three interface positions of the FPU. The first plane of comparison is the P1 position, figure 1b). The second position is a plane between the CLO1 and the LO cryostat window, figure 1d). As a third position we choose a representative plane close to the nominal Focal Plane (FP) of the telescope centered on the chief ray direction of propagation. All the planes for both the simulation and experimental setup were chosen to be centered at a same point belonging to a one common absolute co-ordinate system. Thus simulated and experimental plots are overlapped without any need of trace translation in order to match them. The following results show therefore a remarkable agreement.

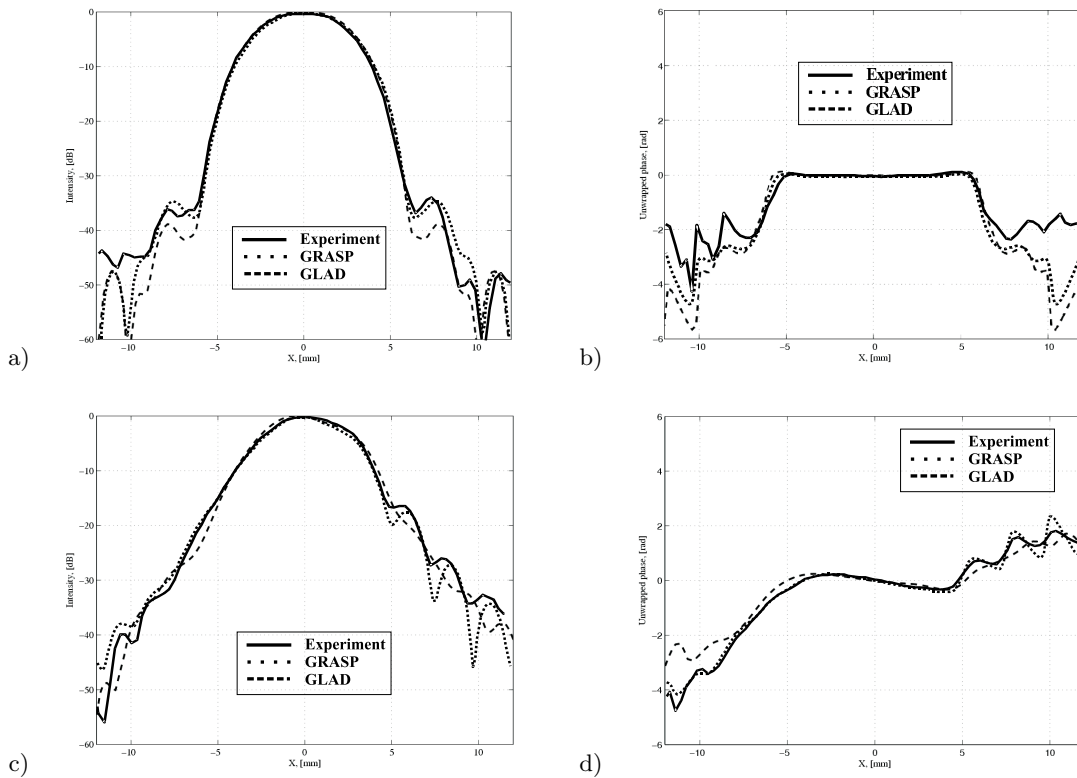


Figure 2. Comparison at P1 position, intensity in dB and phase in radians. a) E-plane intensity; b) E-plane phase; c) H-plane intensity; d) H-plane phase.

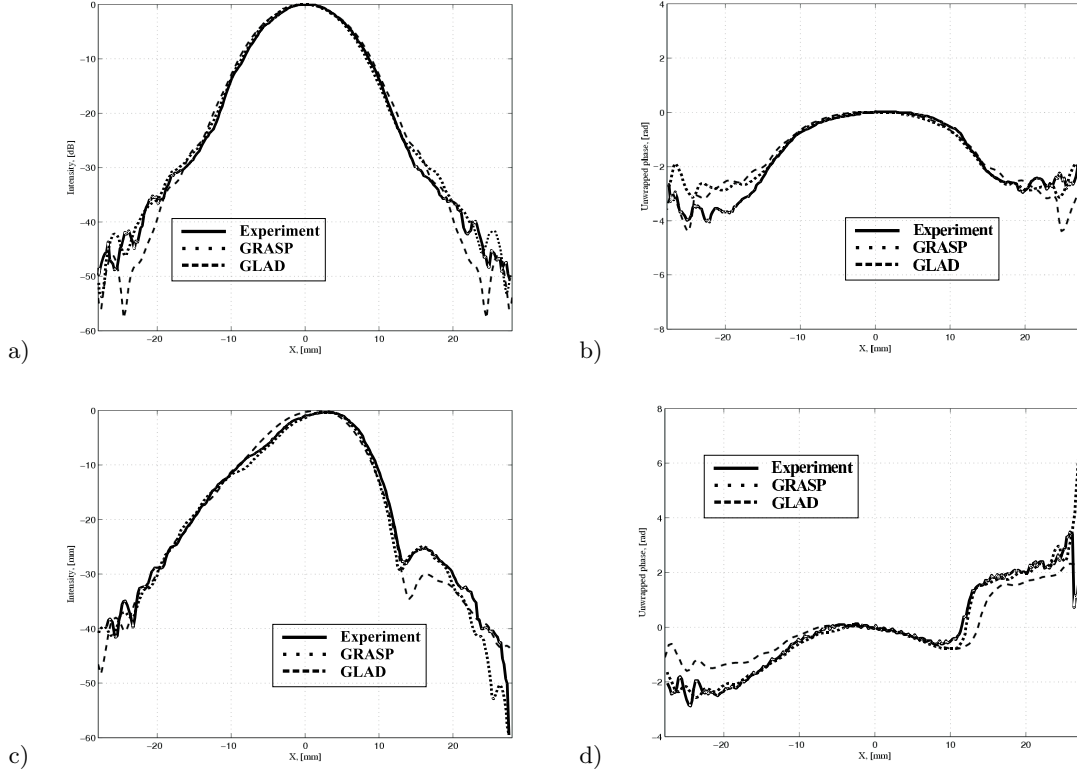


Figure 3. Comparison at LO plane position, intensity in dB and phase in radians. a) E-plane intensity; b) E-plane phase; c) H-plane intensity; d) H-plane phase.

In the end of this section we also show the beam contour levels of the power coupling the Cold Black Body (CBB) and the Hot Black Body (HBB) apertures in the CSA, obtained from GRASP simulations.

In our model the exact rims of the mirrors are modelled on the basis of actual mirror production drawings, arising on a geometrical model as close as possible to the reality. Edge diffraction and truncation affects are therefore properly included in addition to distortions and aberrations imposed by the off-axis reflectors.

Assuming that the input plane is the P2 pupil plane in front of MAM3 (figure 1b)) and the horn being polarized on a direction normal to the telescope on-axis plane, we call the E-plane of measurement the Symmetric plane and the H-plane the Asymmetric plane. Symmetric and Asymmetric also refer to the symmetry sections of the ellipsoidal and paraboloidal rotational mirror surfaces in use in the FPU. In the following figures the co-polar component is shown in the planes previously described at the lower frequency of band 1 being 480 GHz ($0.625\ \mu\text{m}$).

6.1. P1 Position

Formally the P1 position is located at 66.25 mm in front of MAM1 in figure 1b). At this position a beam waist of 3.55 mm is expected[‡], as shown in 2a) and b). From these results is clear visible a strong coma aberration in the Asymmetric plane due to the off-axis paraboloidal mirror MAM1. This effect is also evident in the H-plane phase plot where a cubic phase slope is depicted. This coma feature produce in the beam a so-called "beam-squint" denoting a non-axis peak position of the beam of 0.12 mm through the H-plane⁷.

Simulated and measured data well agree down to -35 dB and -17 dB respectively in the E-plane and in the H-plane. GLAD reliance on plane wave decomposition in the paraxial region, limiting it accuracy in computing

[‡]Waist and beam radius are indicated throughout this paper as the distance from the propagation axis at which the fundamental Gaussian mode field has fallen to $1/e$ of its on-axis value, corresponding at an edge taper of 8.7 dB .

the reflected field from off-axis mirrors. This is particularly evident at greater off-axis distances where the beam divergence is more pronounced.

6.2. LO Position

The LO plane of measurement was taken at 122.3 mm from the LO cryogenic window toward the CLO1 mirror (figure 1d)). Simulation and experiment measurement were performed for the Vertical Polarization (VP) setup shown in figure 1b). In our simulation and experimental setup the beam coming from P1 propagates through a series of flat (BS3, CLO4, CLO2) and curved mirrors (CLO5, CLO3, CLO1) up to the LO cryogenic window where the beam has a waist of 7.5 mm . In the pictures shown in figure 3 a), b), c) and d) we denote again

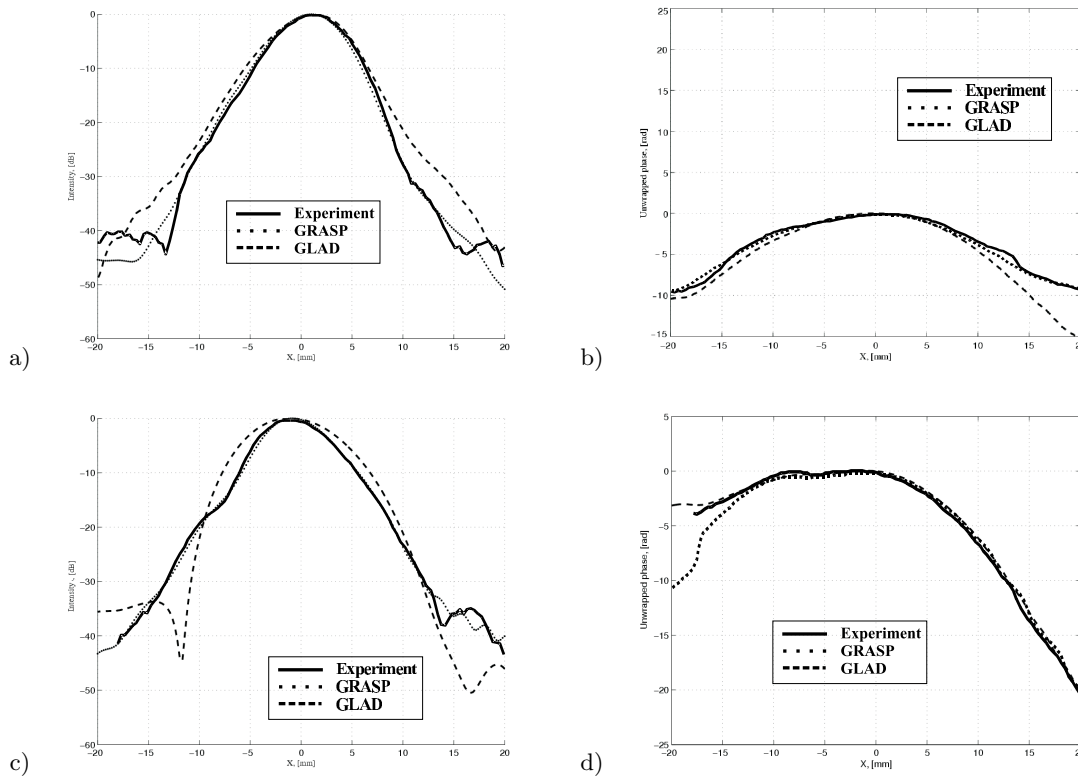


Figure 4. Comparison at the FP position, intensity in dB and phase in radians. a) E-plane intensity; b) E-plane phase; c) H-plane intensity; d) H-plane phase.

aberration features in the Asymmetric plane due to off-axis mirrors in the optical path. However these new off-axis mirrors present a lower off-axis angle compare to MAM1 (90° paraboloid mirror) allowing even GLAD to predict correctly the shape down to -25 dB at the H-plane. A good agreement of the three traces is shown down to -25 dB for the E-plane. The beam squint along the H-plane in this case is more severe being 2.6 mm ⁷. The phase plot still shows a significant tilt characteristic due to coma aberrations. Further, we have to mention that in complex near-field reflector systems, phase errors can be transformed into amplitude errors and vice versa producing unexpectedly results. This is even more evident comparing the beams at the LO window position coming respectively from the HP and the VP MSAs. In fact for the HP beam pattern at the LO window the beam peak is slightly centered on the nominal window axis, due to the possible correctional effect introduced by the additional flat mirror at the position of BS1 in the HP setup. This surface in our model represent the only difference between the VP and HP paths, so it is quite straightforward to think about an effective correctional effect on the P1 beam pattern beam-squint propagating into the CLO unit⁷.

6.3. FP position

The HP MSA beam is now propagated along the entire COA passing through P1 and scattering through 9 more mirrors. The last mirror of the COA (M3 in figure 1a) and c)) used to redirect the out coming beam to the Cassegrain system was not included. The M6 chopper mirror was positioned therefore at the nominal angle of 0° for direct pointing to the telescope. In figure 4 a), b), c) and d) the usual E-plane and H-plane comparisons are shown. Despite the large number of scatterers added in to the system, GRASP and the experimental data agree very well up to -40 dB , illustrating the accuracy at which GRASP simulations can be made. The GLAD result now shows its limitations in accurately modelling a series of off-axis mirrors, which occur in the COA optical path. The beam through the COA has also 3D spatial reflection path changing plane of propagation four times. Despite the fact the beam center is at the same position for the cuts shown in figures 4 a) and c) the real peak is decentered along both the E- and H-planes. The peak position is located slightly closer to the H-plane but offset from the E-plane by -0.7 mm ⁷.

6.4. CSA positions

The CSA is an appendix of the COA which provide two temperature references for the receiver calibration. The two black bodies are visible from the mixer feed according particular angular positions of the M6 chopper mirror. In particular the M6 angle position of 8.4° allow the mixer beam to point the CBB aperture (10K). Positioning

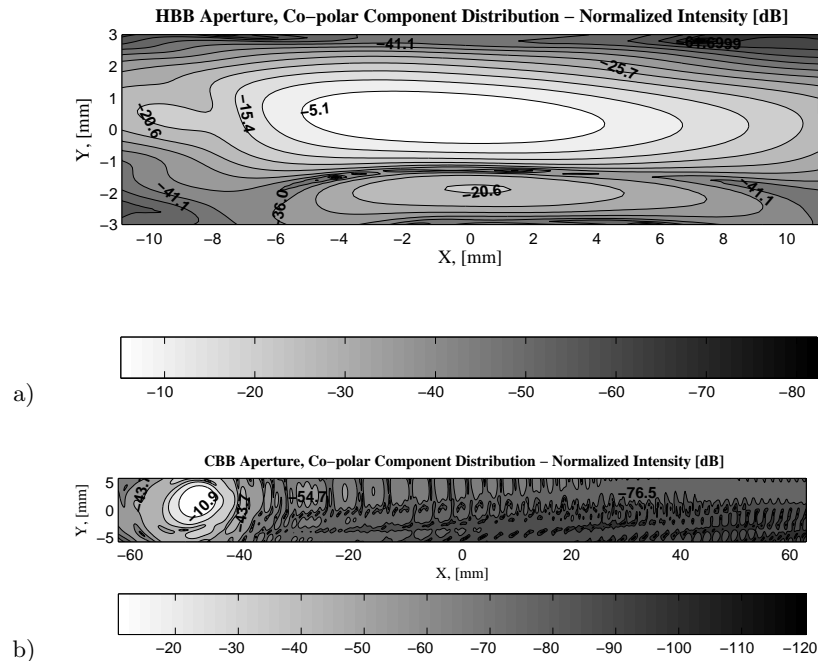


Figure 5. Intensity level contour of the incident beam at the CBB and the HBB in the CSA.

the chopper angle at 10.4° makes the beam scattering through two additional curved (spherical and cylindrical respectively) mirrors in the MSA designed for focusing the beam in the HBB (90K). These preliminary positions of the chopper mirror show that the beam is hitting the black bodies areas in the center with the power levels at the aperture rims around -40 dB . From the simulated data the spillover efficiency for the total power incident on the black body apertures were computed to be 99.91% for the CBB aperture and 99.71% for the HBB aperture. However both of these numbers do not take into account the overall spillover due to all the scatterers in the system. Further studies must be done in order to relate the total power at the mixer and the total system spillover.

7. BAND 1 MSA FIELD MIRROR OPTIMIZATION

As was shown in the preceding section, the beam at the P1 location was aberrated on the asymmetric plane. Using GRASP, an in depth analysis of the resultant fields from each mirror in the MSA was made. It was shown that this particular aberration originated from the MAM2 mirror. This arises from the geometrical design criteria being applied to this optical project. Since at the actual wavelengths the field extends over the mirror surface and since the radius of curvature of the wave front and the mirror do not match, a Phase Error (PE) across the reflector surface is produced ⁷. In addition off-axis mirrors distort the amplitude of the incoming beam ⁸. The main idea in order to optimize the behavior of the MAM2 reflector, was to study a particular PE at the MAM2 incident plane that could produce the desired output beam at the P1 position after reflection at MAM1 reflection figure 6a). In our model a Gaussian Beam (GB) representation of the fields propagated from the feeds was used at the design frequency of $561GHz$ (centre band 1 frequency). The fundamental Gaussian mode was used as an approximation to the corrugated horn feed as the beam coupling efficiency within these two fields is as high as 98%.⁶ As depicted in figure 6a) a GB propagated with a virtual waist of $1.14mm$ from the waist position behind the horn aperture (⁶) for the mixer horn and a GB of $3.55mm$ waist from the P1 position, $66.25mm$ from the MAM1 surface. Referring to the electric fields scattered by MAM1 and MAM3 as \bar{E}_1 and \bar{E}_3 respectively we compute the electric field information for both these beams on the incident plane centered at the incident point of MAM2. In general \bar{E}_i , with $i = 1, 3$, can be described as $\bar{E}_i(x, y) = |\bar{E}_i(x, y)|e^{j\phi_i(x, y)}$ on

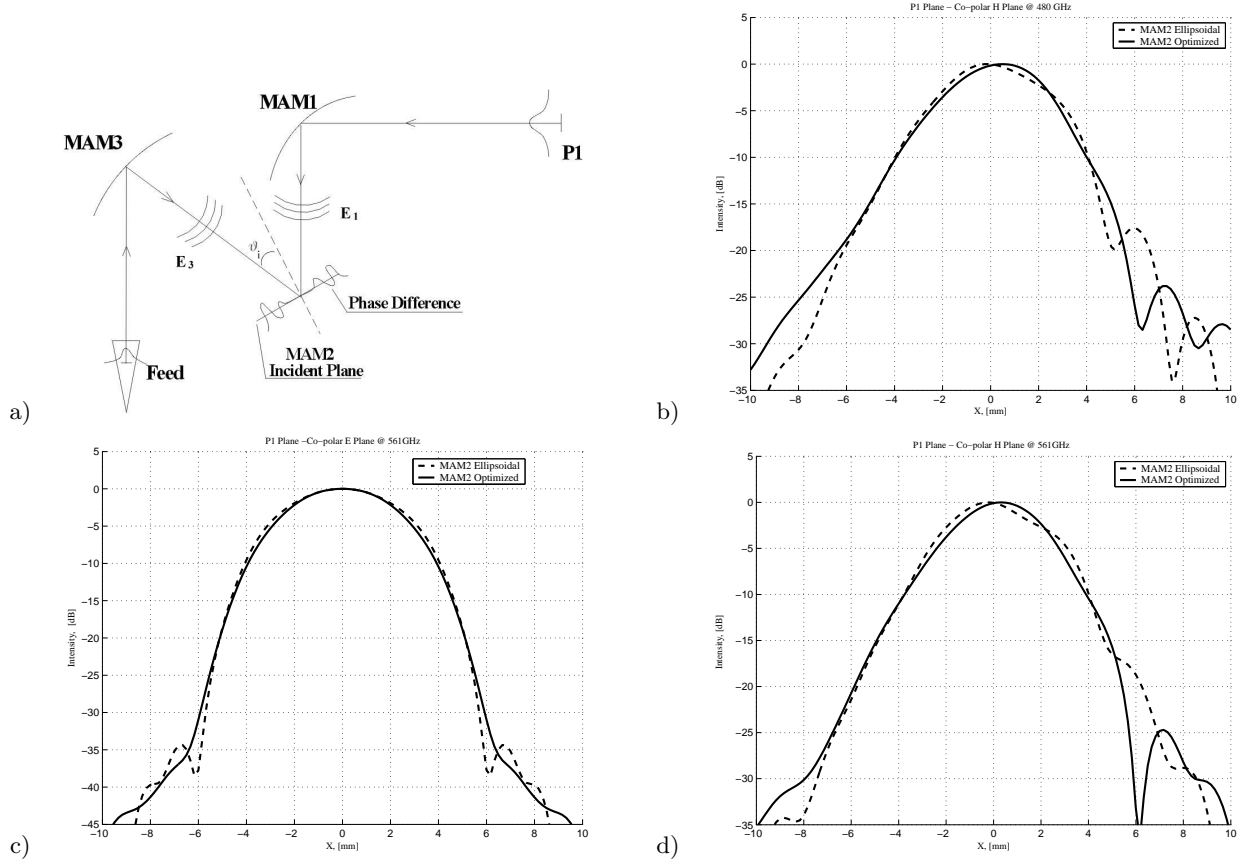


Figure 6. MAM2 Optimization scheme and final result comparisons.

the incident plane tangent at the chief ray incident point on MAM2. We then evaluated the Phase Difference (PD) (or PE), between the two complex fields on the incident plane. However we have to take into account the fact that in the real system the beam reflected from MAM2 has an opposite sense of propagation with respect

to \bar{E}_1 in our model. That implies a change of sign for the phase on the incidence plane, as the \bar{E}_1 beam was incident from the opposite direction. Thus, the phase difference is given by

$$\phi_{diff}(x, y) = (-\phi_1(x, y)) - \phi_3(x, y), \quad \text{On MAM2 Incident Plane.} \quad (3)$$

ϕ_{diff} is now representing the phase transformation properties that allow one to obtain a desired beam at the P1 position. A further step must be considered considering that until now the phase information was expressed in terms of radians. In free space the propagation constant k is equal to $2\pi/\lambda$, where λ is the free space wavelength for the design frequency in use. Thus ϕ_{diff} can be expressed in terms of distances as the phase in general can equal to $\phi = kz$. Finally the shape of the mirror is described with respect to the incident tangent plane by this relation

$$z_{surf}(x, y) = \frac{1}{2} \cdot \frac{\phi_{diff}(x, y)}{k}. \quad (4)$$

$z_{surf}(x, y)$ is now a physical length. The $1/2$ term takes into account the fact that the beam has to traverse the distance from the plane to the curved mirror surface twice.

In figure 6a) b) c) we summaries our GRASP simulation comparisons of the electric field pattern at P1 position with the nominal ellipsoidal MAM2 mirror and the new improved surface placed at the position of MAM2 (centres coinciding) with an inclination equal to the nominal incident angle ϑ_i of 26.56° . The aberration structures present on the right side of the co-polar H-plane are improved introducing the optimized surface. At the design frequency this improvement makes the beam shape more symmetric with a first sidelobe $25dB$ below the main beam. At the lower frequency of band 1, $480GHz$, this sidelobe level is now $7dB$ lower compared with using the nominal MAM2 surface. The improved beam shape at the P1 position also improves power coupling to on axis Gaussian beam [§]. At the design frequency the Gaussian beam coupling efficiency changes from 95.62% to 96.81% using the optimized surface. At the lower frequency this change is small with only an improvement of 0.2% respect the 95.42% using the nominal surface. The beam radius at the edge taper of $8.7dB$ remains $3.55mm$ as expected.

Thus, the beam distortions are minimized although there is still evidence for a coma like aberration. This is due to the large off-axis angle the beam is deflected by at MAM3 and would require a more sophisticated optical configuration involving further mirrors to optimize.

8. CONCLUSIONS

We have discussed the optical verification of the HIFI optics for the Herschel Space Observatory concentrating on the longest wavelength of band 1.

The simulated and experimental measurements made at various output planes in HIFI show remarkable agreement down to the level of $-40dB$. The GRASP simulations, in particular, agree in fine detail with the experimental results with the GLAD predictions slightly less accurate probably due to the approximations and assumptions used within the package. Nonetheless GLAD proves to be successful in predicting the overall characteristics of the beam profile.

Furthermore we present contour plots related to the beam size at the CBB and HBB aperture in the MSA showing that for a particular angular position for M6 the spillover efficiency is extremely high at the black body aperture planes.

We have also shown that a redesign and optimization of the MAM2 mirror could be used to remove distortion and aberrational effects and improve the on-axis beam coupling coefficient of the beam.

ACKNOWLEDGMENTS

The authors would like to acknowledge the support of Enterprise Ireland (Prodex).

[§]The Gaussian beam coupling efficiency represents the fraction of power flowing into an on-axis fundamental Gaussian mode of waist $3.55mm$.

REFERENCES

1. W. Jellema et al, *Performance Characterization and Measurement Results of a Submillimeter-Wave Near-Field Facility for the Heterodyne Instrument for the Far-Infrared*, Proceeding of the 3rd ESA Workshop on Millimeter Wave Technology and Applications, Millilab, Espoo, Finland, May 21-23 2003.
2. B.D. Jackson, K. J. Wildeman, N. D. Whyborn, *The HIFI Focal Plane Unit*, 13th International Symposium on Space Terahertz Technology, pp. 339-348, 26-28 March 2002, Harvard University, Cambridge, Massachusetts, USA.
3. C. Smorenburg, B. Kruizinga and H. Visser, *HIFI Main Optics Design and Analysis*, TNO - TPD, Deft, the Netherlands, 15 January 2001.
4. G. Lawrence, *Optical system analysis with Physical Optics codes*, SPIE no 766-18, O-E/Lase, 1987.
5. K. Pontoppidan, *Technical Description of GRASP8*, TICRA, February 2003.
6. P. F. Goldsmith, *Quasioptical Systems: Gaussian Beam Quasioptical Propagation and Applications*, IEEE Press, 1998.
7. W. Jellema, R. Huisman, M. Candotti, T. Finn, N. Trappe, J. A. Murphy, S. Withington, W. Wild, *Comparison of Near-Field Measurements and Electromagnetic Simulations of the Focal Plane Unit of the Heterodyne Instrument for the Far-Infrared.*, 5th International Conference on Space Optics ICSO2004, Amphithre, Toulouse, France, April 2004.
8. J.A. Murphy, *Distortion of a Simple Gaussian Beam on Reflection from Off-Axis Ellipsoidal Mirrors*, Int. Journal of Inf. & Mill. Waves, Vol. 8, pp. 1165-1187, September 1987.